Lawrence Berkeley National Laboratory

Title
Probing the Electronic Structure of a Photoexcited Solar Cell Dye with Transient X-ray Absorption Spectroscopy

Permalink
https://escholarship.org/uc/item/3zj5n823

Author
Kuiken, Benjamin E. Van

Publication Date
2012-06-06

DOI
10.1021/jz300671e

Peer reviewed

Probing the Electronic Structure of a Photoexcited Solar Cell Dye with Transient X-ray Absorption Spectroscopy

Benjamin E. Van Kuiken †, Nils Huse ‡, Hana Cho ‡, Matthew L. Strader ‡, Michael S. Lynch †, Robert W. Schoenlein ‡, and Munira Khalil *†

† Department of Chemistry, University of Washington, Seattle, Washington 98195, United States
‡ Ultrafast X-ray Science Laboratory, Chemical Sciences Division, Lawrence Berkeley National Laboratory, Berkeley, California 94720, United States

Abstract

This study uses transient X-ray absorption (XA) spectroscopy and time-dependent density functional theory (TD-DFT) to directly visualize the charge density around the metal atom and the surrounding ligands following an ultrafast metal-to-ligand charge-transfer (MLCT) process in the widely used Ru^{II} solar cell dye, $Ru(dcbpy)_2(NCS)_2$ (termed N3). We measure the Ru L-edge XA spectra of the singlet ground ($^1A_1$) and the transient triplet (^3MLCT) excited state of $N3^{4-}$ and perform TD-DFT calculations of 2p core-level excitations, which identify a unique spectral signature of the electron density on the NCS ligands. We find that the Ru 2p, Ru e_g, and NCS π^* orbitals are stabilized by 2.0, 1.0, and 0.6 eV, respectively, in the transient ^3MLCT state of the dye. These results highlight the role of the NCS ligands in governing the oxidation state of the Ru center.

Metal-to-ligand charge-transfer (MLCT) states of transition-metal complexes are widely used to harness solar energy in dye-sensitized solar cells (DSSCs).(1-5) These electronic excited states are generated because absorption of light causes electron transfer from metal d orbitals to π^* orbitals of the surrounding ligands. Visualizing the time-evolving electronic and molecular structure of these fleeting MLCT states is crucial for understanding and controlling fundamental photochemical phenomena and for improving the efficiency of light-harvesting devices. The goal of this study is to map the electron density in the ground and the photoexcited ^3MLCT state of one of the most efficient solar cell dyes, $Ru(dcbpy)_2(NCS)_2$ (termed N3), using picosecond Ru L-edge X-ray absorption (XA) spectroscopy and time-dependent density functional theory (TD-DFT).

Time-resolved XA spectroscopy is an ideal probe of local changes in electronic and molecular structure following photoexcitation of a molecule in solution and has been used to study a wide range of chemical phenomena in transition-metal systems over the past several years.(6-15) Ruthenium L-edge XA spectroscopy involves excitations of Ru 2p core electrons to bound valence states and continuum states above the ionization potential. The Ru 2p states are split by core spin–orbit coupling into the $2p_{3/2}$ and $2p_{1/2}$ levels, giving rise to two main spectral features termed L_3- and L_2-edges, respectively. The spectra are dominated by dipole-allowed transitions from the Ru 2p levels to the unoccupied Ru 4d orbitals. Time-resolved Ru L-edge XA spectroscopy sheds light on how the time-evolving electron density around the Ru atom dictates the course of ultrafast charge-transfer processes in solution.

The N3 dye and similar analogues are integral parts of some of the most successful DSSCs to date. Numerous transient absorption studies have shown that excitation with 400 nm light leads to the formation of a ^1MLCT state that undergoes an ultrafast (<50 fs) intersystem crossing to a

metastable ^{3}MLCT state with a lifetime of 59 ns.(16-21) It is well-known that the electronic structure of the dye molecule critically influences the performance of DSSCs, and quantum chemical calculations have been routinely employed to aid in the engineering of new solar cell dyes.(22-24) In this study, we focus on visualizing the time-evolving local electronic structure of free $N3^{4-}$ in solution.

The Ru L_3-edge XA spectrum of the $^1A_1$ ground state shown in Figure 1a reports on $2p_{3/2} \rightarrow 4d$ core transitions and contains two features labeled B and C. The XA difference spectrum in Figure 1b encodes the changes in the electronic structure at 250 ps following the ultrafast charge transfer from the Ru atom to a dcbpy ligand with 400 nm light. These changes result in the XA spectrum of the transient ^{3}MLCT state (Figure 1a) displaying (i) a new feature A′ at 2837.5 eV, (ii) the main spectral feature B′ shifted to +1.0 eV, and (iii) the feature C′ shifted by +1.4 eV with respect to the ground state. The peak positions of all of the spectral features are listed in Table 1. The time evolution of the difference XA spectrum is shown in the inset of Figure 1b and confirms that the ^{3}MLCT state of $N3^{4-}$ forms within the 70 ps time resolution of the experiment. The XA spectra of the $^1A_1$ and ^{3}MLCT electronic states of $N3^{4-}$ at the Ru L_2-edge, reporting on $2p_{1/2} \rightarrow 4d$ core transitions, mirror the changes observed at the L_3-edge and are shown in Figure S3 of the Supporting Information.
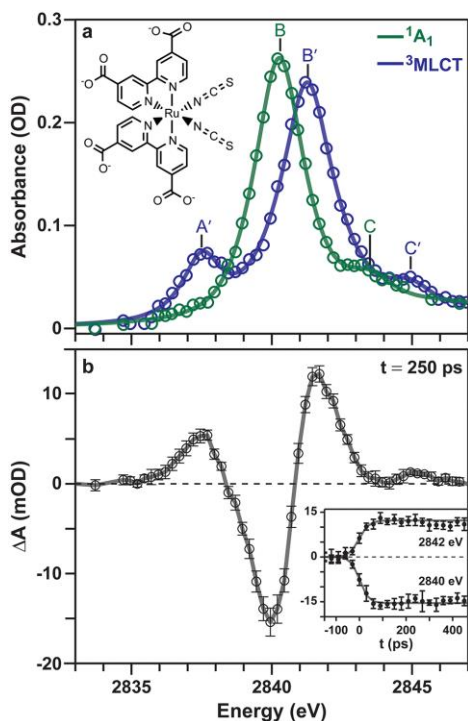

Figure 1. (a) Ru L_3-edge XA spectrum of the $^1A_1$ ground state (green) and transient ^{3}MLCT excited state (blue) of $[Ru(dcbpy)_2(NCS)_2]^{4-}$, termed $N3^{4-}$, where dcbpy = 4,4′-dicarboxylic acid-2,2′-bipyridine in water. The ^{3}MLCT spectrum is constructed from the ground state and the transient difference XA spectrum assuming 18% photoexcitation (see Figure S2 and the associated discussion in the Supporting Information). The solid line is a fit of the data to a sum of pseudo-Voigt line shapes (see Figures S4 and S5, Supporting Information). The structure of the dye is shown in the inset. (b) The difference XA spectrum at 250 ps following photoexcitation of $N3^{4-}$ with 100 fs 400 nm light pulses. The inset shows the difference XA spectra as a function of pump–probe delay (t) recorded at the specified energies. Gray curves represent sigmoidal fits of the time-resolved XA data, revealing an experimental time resolution of ∼70 ps given by the X-ray probe pulse width. The error bars correspond to a 95% confidence interval.

Table 1. Peak Positions (eV) for Peaks in the Experimental and Calculated XA Spectra of the Ground and Excited State of N3^{4-a}

	A(A′)	B(B′)	C(C′)
$^1A_1$		2840.3	2843.5 ± 0.2
$^1A_1$ (DFT)		2840.3	2843.3
^{3}MLCT	2837.5 ± 0.1	2841.3	2844.9 ± 0.2
^{3}MLCT (DFT)	2837.3	2841.0	2844.2

^{a} Error bars represent a 95% confidence interval from a least-squares fitting of each peak. Only uncertainty values ≥0.1 are listed above.

The main features in the L-edge XA spectra of d^6 Ru^{II} and d^5 Ru^{III} complexes are commonly assigned using ligand field theory.(25, 26) If we approximate the symmetry of the N3^{4-} molecule as octahedral, the 4d orbitals would be split into the familiar triply degenerate t_{2g} and doubly degenerate e_g orbitals separated by the ligand-field splitting energy, Δ_o. In the $^1A_1$ ground state, the six electrons assume a low-spin configuration occupying the t_{2g} orbitals. As a result, the peak B in the Ru L$_3$-edge XA spectrum is assigned to transitions from the $2p_{3/2}$ orbitals to the vacant e_g orbitals. In the ^{3}MLCT state of N3^{4-}, one of the Ru 4d electrons is transferred to a dcbpy ligand. The resultant transient Ru^{III} d^5 complex has a vacancy in the t_{2g} orbitals, and we observe a new low-energy peak A′, which is assigned to $2p \rightarrow t_{2g}$ transitions. The peak B′ is the $2p \rightarrow e_g$ transition in the ^{3}MLCT state. On the basis of these assignments, the separation of the A′ and B′ peaks provides a direct measure of a ~3.8 eV ligand-field splitting energy in the ^{3}MLCT state of N3^{4-}. The clear pre-edge C (C′) feature has not been discussed extensively in previously published Ru L-edge spectra and does not have a simple "atomic" interpretation as we discuss below.

With the goal of achieving a detailed molecular-level understanding of the MLCT process in N3^{4-}, we simulated the Ru L$_3$-edge XA spectra of the $^1A_1$ and ^{3}MLCT states using TD-DFT, as shown in Figure 2. TD-DFT calculations were carried out using ORCA and employed the B3LYP functional, the def2-SVP basis set (Sapporo-DK3-TZP for Ru), COSMO for solvation effects, and DKH for scalar relativistic effects.(27-32) Further details are given in the Supporting Information. Each spectral feature in the calculated XA spectrum is comprised of multiple transitions tabulated in Tables S2 and S3 (Supporting Information). We note that the calculated XA spectra are able to reproduce all of the experimentally observed trends in terms of relative peak positions (see Table 1), amplitudes, and shapes. The ab initio calculation of the Ru L$_3$-edge XA spectrum generates maps of the difference densities for each of the core transitions, resulting in the experimentally observed spectral features. The positive part of the difference densities plotted in Figure 2c–g maps the spatial distribution of the core-excited electron for representative transitions. The surfaces plotted in Figure 2c and f show significant electron density at the Ru center and along the metal–ligand bond axes, confirming the e_g character of the orbitals contributing to the final state probed by feature B (B′). The difference density in Figure 2e reveals that the A′ spectral feature probes the t_{2g} orbitals of the Ru atom that are strongly mixed with the NCS ligand orbitals. Finally, the difference electron densities plotted in Figure 2d and g

show that the spectral features C (C′) are direct probes of the NCS π^* orbitals in the ground and excited states of $N3^{4-}$.
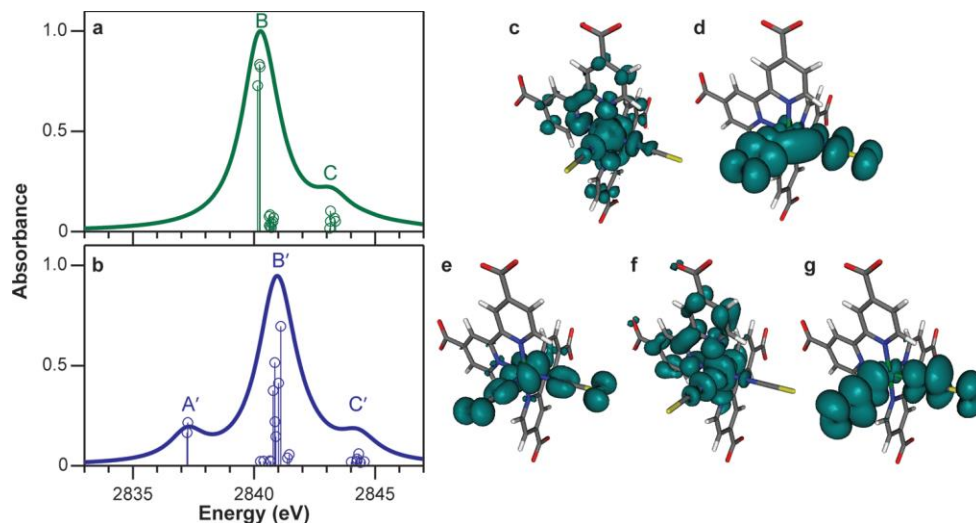

Figure 2. TD-DFT simulations of the Ru L_3-edge XA spectra of the (a) ground $^1A_1$ and (b) transient ^3MLCT states of $N3^{4-}$. The discrete transitions are displayed as circles for each transition with a nonzero oscillator strength and have been convoluted with a Voigt line shape consisting of a 1.75 eV Lorentzian width and a 0.4 eV Gaussian broadening to account for the Ru 2p core–hole lifetime and the resolution of the monochromator, respectively. The calculated spectra are shifted by −2.85 eV to align the feature B of the $^1A_1$ state with the experimental spectrum in Figure 1a. (c–g) Positive part of the difference densities are shown for transitions representative of each of the spectral features. The negative portion of the difference density is concentrated at the Ru core and is not visible.

The combination of time-resolved XA measurements and TD-DFT simulations of the Ru L_3-edge provide a detailed description of the electronic and molecular structure of $^1A_1$ ground and transient ^3MLCT excited states of $N3^{4-}$, as detailed in Figure 3. Figure 3a shows the highest occupied molecular orbital (HOMO) for the $^1A_1$ and ^3MLCT states of $N3^{4-}$. Exciting the $^1A_1$ state with a 400 nm photon depopulates the HOMO orbital containing Ru t_{2g} and NCS π^* character. Following ultrafast intersystem crossing, the excited electron density resides in the HOMO of the ^3MLCT state localized on one dcbpy ligand, as shown in Figure 3a. The ultrafast photoexcitation process leaves a vacancy in the Ru t_{2g} orbitals, giving rise to the new peak A′ in the ^3MLCT L_3-edge spectrum (Figure 1a). A comparison of the difference density plotted in Figure 2e and the HOMO of the $^1A_1$ state in Figure 3a reveals that the A′ feature is a probe of the HOMO vacated upon MLCT excitation. The observation of strong orbital mixing in the HOMO suggests that the ^3MLCT state of $N3^{4-}$ is not a pure Ru^{III} state as the MLCT excitation removes electron density from both metal and NCS ligand orbitals. Our TD-DFT results reveal that the molecular orbital contributing most significantly to the intensity of the A′ transition in the calculated XA spectrum has Mulliken populations of 0.6 and 0.2 for Ru and NCS, respectively (see MO 177β in Figure S7, Supporting Information), and calculated Mulliken charges confirm the loss of electron density on the NCS ligands following the formation of the ^3MLCT state (Table S1, Supporting Information). The mixing between the Ru and NCS orbitals observed in this study agrees with photoelectron spectroscopy of the ground state of N3 and confirms previous theoretical predictions.(33, 34)
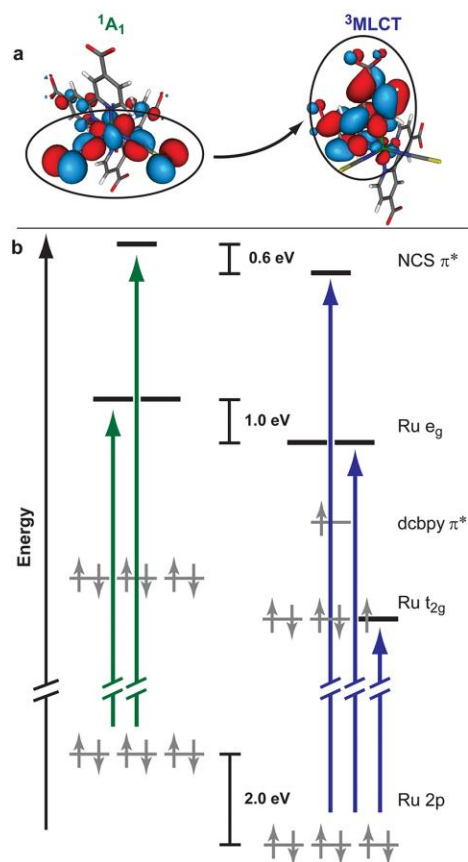
Figure 3. Electronic structure of N3^{4-} in its $^{1}A_1$ (left) and ^{3}MLCT (right) states as revealed by time-resolved Ru L$_3$-edge XA spectroscopy and quantum chemical calculations. (a) HOMO orbitals of N3^{4-} in the singlet and triplet states. The HOMO in the ground state is a mixture of Ru 4d and NCS $\pi*$ orbitals. The HOMO in the triplet state is localized on the one of the dcbpy ligands. (b) Orbital structure of N3^{4-} probed by Ru L$_3$-edge XA spectroscopy assuming octahedral symmetry. Orbitals that give rise to peaks in the XA spectra are shown in bold with green transitions for the singlet and blue transitions for the triplet state. The energetic shifts in the orbitals derived from time-evolving spectral features are shown in the center column.

It is important to note that the experimentally measured spectral shifts in features B and C following 400 nm photoexcitation can originate from changes in the binding energies of the 2p electrons and/or shifts in the valence orbital energies between the $^{1}A_1$ ground and transient ^{3}MLCT excited states of N3^{4-}. By fitting the absorption edge, we determined that the Ru 2p ionization energy increases by 2.0 eV for the ^{3}MLCT state. This agrees well with our DFT calculations, where the average orbital energy for Ru 2p electrons in the ^{3}MLCT state lies 1.5 eV below its ground-state value. The stabilization of the 2p orbitals in the triplet state relative to that for the singlet ground state results from a decrease in shielding concomitant with the decrease in electron density at the Ru atom and is shown schematically in Figure 3b.

We measure a +1.0 eV shift in the transition energy of the B (B′) feature following photoexcitation, which is attributed to a −2.0 eV shift in the 2p core levels and a 1.0 eV decrease in the energy of the Ru e$_g$ orbitals in the ^{3}MLCT state of N3^{4-}. The shift in energy of the Ru e$_g$ orbitals is a complex function of electrostatic and geometric factors. The 400 nm MLCT transition removes electron density at the Ru atom, decreasing the shielding of the e$_g$ orbitals from the nuclear charge and reducing electron–electron repulsion. While these stabilizing

electrostatic effects dominate, the MLCT excitation also results in a 0.04 Å decrease of the average Ru–N_{NCS} distance, which should slightly destabilize the Ru e_g orbitals. We measure a +1.4 eV shift in the transition energy of the C (C′) feature following photoexcitation and attribute it to a 0.6 eV relaxation of the NCS π^* orbitals in the ^{3}MLCT state of N3^{4-} after accounting for the 2p core level shift. As discussed earlier, the 400 nm MLCT excitation removes electron density from both metal and NCS ligand orbitals. The subsequent decrease in the anionic character of the NCS ligands stabilizes their π^* orbitals, as shown in Figure 3b. Our results show how the C (C′) spectral feature in the Ru L_3-edge XA spectrum of N3^{4-} tracks the charge depletion and rearrangement of electron density on the NCS ligands during the MLCT excitation.

It is instructive to compare our time-resolved Ru L_3-edge XA spectroscopy results on the solar cell dye N3 to similar measurements on [Ru(bpy)$_3$]$^{2+}$ performed by Chergui and co-workers.(35) Notably, the Ru L_3-edge spectra of [Ru(bpy)$_3$]$^{2+}$ do not show the spectral feature C (C′) that arises from transitions to the π^* orbitals of the NCS ligands in N3. We note that the feature labeled C in ref 35 is a post-edge feature arising from multiple scattering effects, not to be confused with the pre-edge feature labeled C in Figure 1a. The stabilization of the 2p core levels in the ^{3}MLCT state of [Ru(bpy)$_3$]$^{2+}$ by 1.8 eV is similar to the 2.0 eV value measured for N3^{4-} in this study. Ru L-edge spectroscopy of [Ru(bpy)$_3$]$^{2+}$ predicted a ~0.03 Å decrease in the Ru–N bond distances for the ^{3}MLCT state. This differs from the case of N3^{4-}, where the DFT calculations predict no change in the Ru–N_{dcbpy} bond lengths upon photoexcitation. Recently Zhang et al. performed a complementary time-resolved XA experiment at the Ru K-edge on N3 adsorbed on TiO$_2$ nanoparticles.(8) They reported a 0.06 Å decrease in the Ru–N_{NCS} bond distances and little change in the Ru–N_{dcbpy} bond distances in the N3$^+$ complex following photoinduced charge injection into TiO$_2$. Although the ^{3}MLCT state of N3^{4-} probed in our experiment is different from that of the N3$^+$ complex, the geometry changes upon photoexcitation predicted by our DFT simulations agree closely with the results from the Ru K-edge experiment.

The success of TD-DFT to qualitatively reproduce the equilibrium and transient XA spectra of N3^{4-} in solution builds on recent theoretical studies that have employed methods rooted in Kohn–Sham DFT for simulating Ru L-edge XA spectra.(36, 37) The choice of TD-DFT for calculating L-edge XA spectra of second-row transition-metal complexes requires careful consideration of multiplet and spin–orbit effects and warrants some discussion. The energetic and spatial separation between the 2p and 4d orbitals of the second-row transition metals substantially weakens the p–d exchange interaction, and the L-edge spectra are not dominated by transitions arising from multiplet effects.(38) Campbell et al. applied spin-free DFT using the Z + 1 approximation to interpret the time-resolved Ru L_3-edge XA spectra of [Ru(bpy)$_3$]$^{2+}$.(36) More recently, ground-state orbitals from two-component relativistic calculations were used to construct initial and core-excited states by Koopman-style excitations to simulate and interpret the $L_{2,3}$-edges for several Ru^{II} and Ru^{III} complexes.(37) Both of these approaches were able to reproduce the experimentally observed features, suggesting that multiplet effects in Ru $L_{2,3}$-edge spectra are weak. Our simulations also neglect 4d spin–orbit coupling, but ligand-field multiplet calculations have shown that inclusion of 4d spin–orbit coupling has a very slight effect on peak amplitudes and positions in the Ru L_3-edge spectrum.(39) In the case of the d^5 molecule, [Ru(NH$_3$)$_6$]Cl$_3$, 4d spin–orbit coupling affects only the partially occupied t_{2g} orbitals, shifting the transition energy by +0.13 eV relative to the spin-free value.(25) Because this energy shift is

well below the resolution of our experiment, neglect of spin–orbit coupling has little impact on the interpretation of our experimental spectra using TD-DFT simulations. This is evident from the excellent agreement of our experimental and calculated L_3-edge XA spectra (see Figures 1a and 2a,b and Table 1).

Our ability to design molecules and materials for solar energy capture and conversion relies on the development of new quantitative experimental tools that can track time-evolving electron density at high spatial and temporal resolution. In this study, the combination of ultrafast X-ray absorption spectroscopy and TD-DFT provides a detailed understanding of the time-evolving electron density and molecular structure of the transient ^{3}MLCT state in the widely used solar cell dye molecule, N3^{4-}, in solution. In summary, core-level transitions of the Ru 2p electrons to the Ru 4d orbitals probe the mixing of the metal and the NCS ligand orbitals. Following the 400 nm ultrafast MLCT excitation of N3^{4-}, the dye relaxes to a ^{3}MLCT state indicated by the appearance of the A′ feature in the XA spectrum. The ultrafast transfer of electron density from the Ru atom and the NCS ligands to one of the dcbpy ligands leads to a 2.0 and 1.0 eV stabilization of the Ru 2p and e_g orbitals, respectively. The TD-DFT simulation of the Ru L_3-edge XA spectrum identifies the molecular origin of spectral feature C (C′), which directly tracks the loss of electron density from the NCS ligands during the ultrafast MLCT process. This investigation yields important new insights on the influence of the NCS ligand on charge-transfer and dye regeneration efficiencies in DSSCs. The multielectron transfer mechanism by which the dye is regenerated with the I^-/I_3^- redox couple in a solar cell is still unclear.(40-42) Our results demonstrate that the charge density on the NCS ligands modulates the oxidation state of the N3 dye, which provides a microscopic explanation for the superior efficiency of Ru^{II} dyes containing the NCS ligands. We identify the spectral feature C (C′) in the Ru L-edge XA spectrum as a sensitive NCS-ligand-specific probe, which can be used to monitor transient structural dynamics of the dye regeneration process and aid in the design and engineering of new DSSCs at the molecular level.

Supporting Information
Materials; experimental methods; computational details; transient XA at the Ru L_2-edge of N3^{4-}; fits of XA data for the Ru L_3-edge of N3^{4-}; Mulliken charges from DFT calculations; Cartesian coordinates for optimized geometries of N3^{4-}; and table of TD-DFT transitions and contributing orbitals. This material is available free of charge via the Internet at http://pubs.acs.org.

⊥ Author Present Address
Max Planck Research Department for Structural Dynamics at the University of Hamburg, 22607 Hamburg, Germany.

Acknowledgment

References

1. Grätzel, M.Solar Energy Conversion by Dye-Sensitized Photovoltaic Cells Inorg. Chem. 2005, 44, 6841– 6851

2. Grätzel, M.Recent Advances in Sensitized Mesoscopic Solar Cells Acc. Chem. Res. 2009, 42, 1788– 1798

3. Anderson, N. A.; Lian, T.Ultrafast Electron Transfer at the Molecule–Semiconductor Nanoparticle Interface Annu. Rev. Phys. Chem. 2005, 56, 491– 519

4. Ardo, S.; Meyer, G. J.Photodriven Heterogeneous Charge Transfer with Transition-Metal Compounds Anchored to TiO_2 Semiconductor Surfaces Chem. Soc. Rev. 2009, 38, 115– 164

5. Hagfeldt, A.; Boschloo, G.; Sun, L.; Kloo, L.; Pettersson, H.Dye-Sensitized Solar Cells Chem. Rev. 2010, 110, 6595– 6663

6. Chen, L. X.Probing Transient Molecular Structures in Photochemical Processes Using Laser-Initiated Time-Resolved X-ray Absorption Spectroscopy Annu. Rev. Phys. Chem. 2005, 56, 221– 254

7. Chen, L. X.; Zhang, X.; Wasinger, E. C.; Lockard, J. V.; Stickrath, A. B.; Mara, M. W.; Attenkofer, K.; Jennings, G.; Smolentsev, G.; Soldatov, A.X-ray Snapshots for Metalloporphyrin Axial Ligation Chem. Sci. 2010, 1, 642– 650

8. Zhang, X.-Y.; Smolentsev, G.; Guo, J.-C.; Attenkofer, K.; Kurtz, C.; Jennings, G.; Lockard, J. V.; Stickrath, A. B.; Chen, L.-X.Visualizing Interfacial Charge Transfer in Ru-Dye-Sensitized TiO_2 Nanoparticles Using X-ray Transient Absorption Spectroscopy J. Phys. Chem. Lett. 2011, 2, 628– 632

9. Chergui, M.Picosecond and Femtosecond X-ray Absorption Spectroscopy of Molecular Systems Acta Crystallogr., Sect. A 2010, A66, 229– 239

10. Bressler, C.; Chergui, M.Molecular Structural Dynamics Probed by Ultrafast X-ray Absorption Spectroscopy Annu. Rev. Phys. Chem. 2010, 61, 263– 282

11. Khalil, M.; Marcus, M. A.; Smeigh, A. L.; McCusker, J. K.; Chong, H. H. W.; Schoenlein, R. W.Picosecond X-ray Absorption Spectroscopy of a Photoinduced Iron(II) Spin Crossover Reaction in Solution J. Phys. Chem. A 2006, 110, 38– 44

12. Huse, N.; Cho, H.; Hong, K.; Jamula, L.; de Groot, F. M. F.; Kim, T. K.; McCusker, J. K.; Schoenlein, R. W.Femtosecond Soft X-ray Spectroscopy of Solvated Transition-Metal Complexes: Deciphering the Interplay of Electronic and Structural Dynamics J. Phys. Chem. Lett. 2011, 2, 880– 884

13. Huse, N.; Kim, T. K.; Jamula, L.; McCusker, J. K.; de Groot, F. M. F.; Schoenlein, R. W.Photoinduced Spin-State Conversion in Solvated Transition Metal Complexes Probed via Time-Resolved Soft X-ray Spectroscopy J. Am. Chem. Soc. 2010, 132, 6809– 6816

14. Lee, T.; Jiang, Y.; Rose-Petruck, C. G.; Benesch, F.Ultrafast Tabletop Laser-Pump–X-ray Probe Measurement of Solvated $Fe(CN)_6^{4-}$ J. Chem. Phys. 2005, 122, 084501– 084508

15. Chen, J.; Rentzepis, P. M.Evolution of Transient Structures in Solids and Liquids by Means of Time Resolved X-ray Diffraction and X-ray Absorption Fine Structure Adv. Multi-Photon Processes Spectrosc. 2010, 19, 117– 183

16. Benkö, G.; Kallioinen, J.; Korppi-Tommola, J. E. I.; Yartsev, A. P.; Sundström, V.Photoinduced Ultrafast Dye-to-Semiconductor Electron Injection from Nonthermalized and Thermalized Donor States J. Am. Chem. Soc. 2001, 124, 489– 493

17. Asbury, J. B.; Ellingson, R. J.; Ghosh, H. N.; Ferrere, S.; Nozik, A. J.; Lian, T.Femtosecond IR Study of Excited-State Relaxation and Electron-Injection Dynamics of $Ru(dcbpy)_2(NCS)_2$ in Solution and on Nanocrystalline TiO_2 and Al_2O_3 Thin Films J. Phys. Chem. B 1999, 103, 3110– 3119

18. Tachibana, Y.; Moser, J. E.; Grätzel, M.; Klug, D. R.; Durrant, J. R.Subpicosecond Interfacial Charge Separation in Dye-Sensitized Nanocrystalline Titanium Dioxide Films J. Phys. Chem. 1996, 100, 20056– 20062

19. Bräm, O.; Messina, F.; El-Zohry, A. M.; Cannizzo, A.; Chergui, M.Polychromatic Femtosecond Fluorescence Studies of Metal–Polypyridine Complexes in Solution Chem. Phys. 2012, 393, 51– 57

20. Bhasikuttan, A. C.; Okada, T.Excited-State Relaxation Dynamics of $Ru(dcbpy)_2(NCS)_2$, Studied by Fluorescence Upconversion Spectroscopy J. Phys. Chem. B 2004, 108, 12629– 12632

21. Nazeeruddin, M. K.; Kay, A.; Rodicio, I.; Humphry-Baker, R.; Mueller, E.; Liska, P.; Vlachopoulos, N.; Graetzel, M.Conversion of Light to Electricity by *cis*-X$_2$Bis(2,2′-bipyridyl-4,4′-dicarboxylate)ruthenium(II) Charge-Transfer Sensitizers (X = Cl⁻, Br⁻, I⁻, CN⁻, and SCN⁻) on Nanocrystalline Titanium Dioxide Electrodes J. Am. Chem. Soc. 1993, 115, 6382– 6390

22. Fantacci, S.; De, A. F.A Computational Approach to the Electronic and Optical Properties of Ru(II) and Ir(III) Polypyridyl Complexes: Applications to DSC, OLED and NLO Coord. Chem. Rev. 2011, 255, 2704– 2726

23. Barolo, C.; Nazeeruddin, M. K.; Fantacci, S.; Di, C. D.; Comte, P.; Liska, P.; Viscardi, G.; Quagliotto, P.; De, A. F.; Ito, S.Synthesis, Characterization, and DFT-TDDFT Computational Study of a Ruthenium Complex Containing a Functionalized Tetradentate Ligand Inorg. Chem. 2006, 45, 4642– 4653

24. Nazeeruddin, M. K.; De Angelis, F.; Fantacci, S.; Selloni, A.; Viscardi, G.; Liska, P.; Ito, S.; Takeru, B.; Graetzel, M.Combined Experimental and DFT-TDDFT Computational Study of Photoelectrochemical Cell Ruthenium Sensitizers J. Am. Chem. Soc. 2005, 127, 16835– 16847

25. Sham, T. K.X-ray Absorption Spectra of Ruthenium L Edges in Hexaammineruthenium Trichloride J. Am. Chem. Soc. 1983, 105, 2269– 2273

26. de Groot, F.; Kotani, A. Core Level Spectroscopy of Solids; CRC Press: Boca Raton, FL, 2008.

27. Neese, F.The Orca Program System Wiley Interdiscip. Rev.: Comput. Mol. Sci. 2012, 2, 73– 78

28. Becke, A.A New Mixing of Hartree-Fock and Local Density Functional Theories J. Chem. Phys. 1993, 98, 1372– 1377

29. Weigend, F.; Ahlrichs, R.Balanced Basis Sets of Split Valence, Triple Zeta Valence and Quadruple Zeta Valence Quality for H to Rn: Design and Assessment of Accuracy Phys. Chem. Chem. Phys. 2005, 7, 3297– 3305

30. Klamt, A.; Schueuermann, G.Cosmo: A New Approach to Dielectric Screening in Solvents with Explicit Expressions for the Screening Energy and Its Gradient J. Chem. Soc., Perkin Trans. 2 1993, 799– 805

31. Noro, T.; Sekiya, M.; Koga, T.; Saito, S. L.Relativistic Contracted Gaussian-Type Basis Functions for Atoms K through Xe Chem. Phys. Lett. 2009, 481, 229– 233

32. Neese, F.Calculation of Electric-Field Gradients Based on Higher-Order Generalized Douglas–Kroll Transformations J. Chem. Phys. 2005, 122, 204107– 204116

33. Rensmo, H.; Södergren, S.; Patthey, L.; Westermark, K.; Vayssieres, L.; Kohle, O.; Brühwiler, P. A.; Hagfeldt, A.; Siegbahn, H.The Electronic Structure of the *cis*-Bis(4,4′-dicarboxy-2,2′-bipyridine)-bis(isothiocyanato)ruthenium(II) Complex and Its Ligand 2,2′-Bipyridyl-4,4′-dicarboxylic Acid Studied with Electron Spectroscopy Chem. Phys. Lett. 1997, 274, 51– 57

34. De Angelis, F.; Fantacci, S.; Selloni, A.Time-Dependent Density Functional Theory Study of the Absorption Spectrum of $[Ru(4,4′-COOH-2,2′-bpy)_2(NCS)_2]$ in Water Solution: Influence of the pH Chem. Phys. Lett. 2004, 389, 204– 208

35. Gawelda, W.; Johnson, M.; de, G. F. M. F.; Abela, R.; Bressler, C.; Chergui, M.Electronic and Molecular Structure of Photoexcited $[Ru^{II}(bpy)_3]^{2+}$ Probed by Picosecond X-ray Absorption Spectroscopy J. Am. Chem. Soc. 2006, 128, 5001– 5009

36. Campbell, L.; Mukamel, S.Simulation of X-ray Absorption near Edge Spectra of Electronically Excited Ruthenium Tris-2,2′-bipyridine J. Chem. Phys. 2004, 121, 12323– 12333

37. Alperovich, I.; Smolentsev, G.; Moonshiram, D.; Jurss, J. W.; Concepcion, J. J.; Meyer, T. J.; Soldatov, A.; Pushkar, Y.Understanding the Electronic Structure of 4d Metal Complexes: From Molecular Spinors to L-Edge Spectra of a Di-Ru Catalyst J. Am. Chem. Soc. 2011, 133, 15786– 15794

38. de Groot, F.High-Resolution X-ray Emission and X-ray Absorption Spectroscopy Chem. Rev. 2001, 101, 1779– 1808

39. de Groot, F. M. F.Differences between L_3 and L_2 X-ray Absorption Spectra of Transition Metal Compounds J. Chem. Phys. 1994, 101, 6570– 6576

40. Nyhlen, J.; Boschloo, G.; Hagfeldt, A.; Kloo, L.; Privalov, T.Regeneration of Oxidized Organic Photo-Sensitizers in Grätzel Solar Cells: Quantum-Chemical Portrait of a General Mechanism ChemPhysChem 2010, 11, 1858– 1862

41. Privalov, T.; Boschloo, G.; Hagfeldt, A.; Svensson, P. H.; Kloo, L.A Study of the Interactions between I^-/I_3^- Redox Mediators and Organometallic Sensitizing Dyes in Solar Cells J. Phys. Chem. C 2008, 113, 783– 790

42. Schiffmann, F.; VandeVondele, J.; Hutter, J.; Urakawa, A.; Wirz, R.; Baiker, A.An Atomistic Picture of the Regeneration Process in Dye Sensitized Solar Cells Proc. Natl. Acad. Sci. U.S.A. 2010, 107, 4830– 4833

DISCLAIMER